

# Chapter 1

## Material Design Considerations Based on Thermoelectric Quality Factor

Heng Wang, Yanzhong Pei, Aaron D. LaLonde and G. Jeffery Snyder

**Abstract** In this chapter several aspects of the electronic and phonon structure are considered for the design and engineering of advanced thermoelectric materials. For a given compound, its thermoelectric figure of merit,  $zT$ , is fully exploited only when the free carrier density is optimized. Achieving higher  $zT$  beyond this requires the improvement in the material quality factor  $B$ . Using experimental data on lead chalcogenides as well as examples of other good thermoelectric materials, we demonstrate how the fundamental material parameters: effective mass, band anisotropy, deformation potential, and band degeneracy, among others, impact the thermoelectric properties and lead to desirable thermoelectric materials. As the quality factor  $B$  is introduced under the assumption of acoustic phonon (deformation potential) scattering, a brief discussion about carrier scattering mechanisms is also included. This simple model with the use of an effective deformation potential coefficient fits the experimental properties of real materials with complex structures and multi-valley Fermi surfaces remarkably well—which is fortunate as these are features likely found in advanced thermoelectric materials.

### 1.1 Introduction

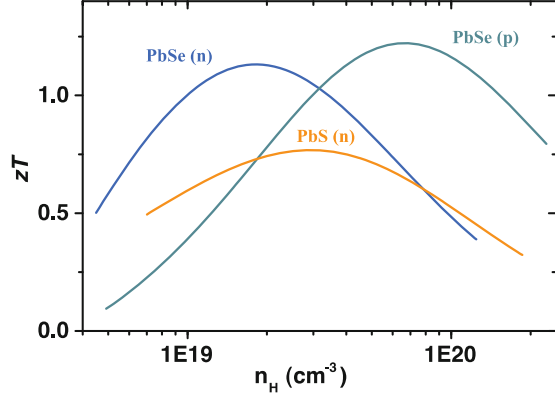
At the material level of thermoelectric research, the overriding goal is to achieve higher figure of merit  $zT = S^2\sigma T/\kappa$ . It is easy to show for semiconductors using the simple transport model for semiconductors, that most of these properties: the Seebeck coefficient  $S$ , the electric conductivity  $\sigma$  and the electronic component of thermal conductivity  $\kappa_e$  for a given material are each functions of carrier

---

H. Wang (✉) · Y. Pei · A. D. LaLonde · G. J. Snyder  
Department of Materials Science, California Institute of Technology, Pasadena, CA 91125, US  
e-mail: hengwang@caltech.edu

G. J. Snyder  
e-mail: jsnyder@caltech.edu

**Fig. 1.1**  $zT$  at 800 K as a function of carrier density for a few lead chalcogenides. The highest  $zT$  is achieved at a specific carrier density, which is different even for such similar compounds or the same compound with different doping type



concentration (or more fundamentally, chemical potential  $\zeta$ ). This means the full potential of a material as thermoelectrics or, the highest  $zT$ , will only be exploited when the carrier concentration is optimized (Fig. 1.1).

The merit of a semiconducting compound as a thermoelectric material can be evaluated without exploring the entire carrier density range but through several fundamental parameters. Through history of thermoelectrics the combination of such parameters has been pointed out in similar forms by different researchers. It has first been discussed in 1959 by Chasmar and Stratton [1, 2] and referred to as the “material factor”  $\beta$  where:

$$\beta = (k_B/e)^2 T \sigma_c / \kappa_L \propto m^{*3/2} \mu_c T / \kappa_L \quad (1.1)$$

It was rewritten by Goldsmid [3] and Nolas et al. [4] as (in SI units):

$$\beta = 5.745 \times 10^{-6} m^{*3/2} \mu_c / \kappa_L T^{5/2} \quad (1.2)$$

The same quantity has been called the “B factor” by Mahan [5]. Additionally, since the electronic properties and lattice thermal conductivity are often considered independently tunable, the electronic part of  $\beta$  or  $B$  is also stressed for example by Slack [6] when discussing the criteria for good thermoelectric materials as the “weighed mobility”  $U$

$$U = \mu_0 m^{*3/2} \quad (1.3)$$

In each of the above expressions,  $m^*$  is the effective mass (in  $m_e$ )  $\mu_c$  is the mobility value at nondegenerate, classical limit and  $\mu_0$  is the mobility value in the purest samples, i.e. when the material is defect free, the carrier concentration is low and the chemical potential  $\zeta \ll 0$ .

These expressions, having their merit in focusing on fundamental material properties, have been serving as a guideline for searching for new thermoelectric materials. The best thermoelectric compounds used at high temperatures have the largest  $B$  of

**Fig. 1.2**  $zT$  as a function of reduced chemical potential  $\eta(\zeta/k_B T)$  for different quality factor  $B$

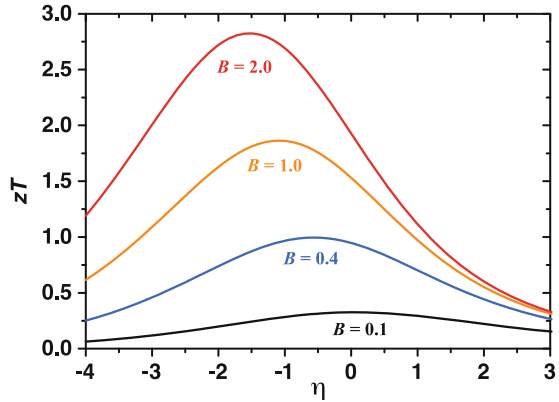
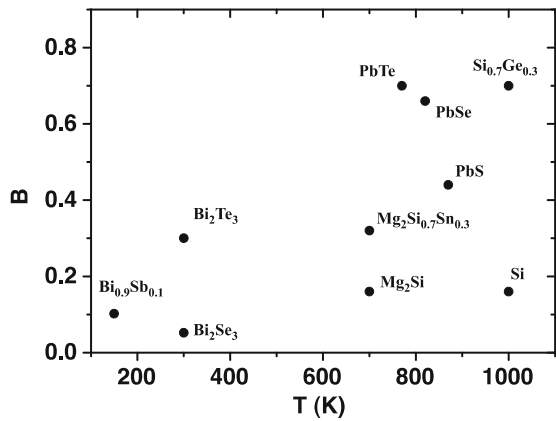


**Fig. 1.3** Quality factor  $B$  for a few thermoelectric compounds at their respective application temperatures



around 1, whereas for room temperature or cryogenic applications the best materials only have  $B$  below half of this value (Figs. 1.2, 1.3).

There are however a few ambiguities in the above expression of  $\beta$  (or  $B$  or  $U$ ) that can possibly be improved for thermoelectric research. First, one underlying assumption that connects these material parameters to highest  $zT$  is that the carrier scattering mechanism is unchanged [1, 6]. Since all practical thermoelectrics are heavily doped, degenerate semiconductors, the scattering mechanism of carriers in this doping region is not necessarily the same as when the crystal lattice is perfect. In other words, to accurately evaluate  $\beta$ ,  $\mu_0$  should be extrapolated from mobilities of properly doped materials of thermoelectric interest to its classical limit rather than using the highest measured mobility on an undoped sample. Otherwise  $\beta$  would be underestimated if the nondegenerate mobility were limited by other mechanisms whose influence would fade away as the carrier concentration is increased (for instance the bipolar effect).

Second, the appearance of  $\beta$  being a product of  $\mu_0$  and  $m^{*3/2}$  may lead to the wrong impression that larger effective mass  $m^*$  is beneficial for thermoelectrics, while actually for most scattering mechanisms  $\mu_0$  is also a function of  $m^*$ . Most importantly when acoustic phonon scattering is dominant, which is usually a good assumption for all good thermoelectric materials above room temperature,  $\mu_0$  will decrease with  $m^{*5/2}$ , which clearly indicates that for similar compounds, a smaller  $m^*$  actually will lead to a larger  $U$  (and  $\beta$  or  $B$ ) [7]. In fact such conclusion had been made by Chasmar and Stratton [1] as well as Goldsmid [2]. But still the current form of  $\beta$  is used to keep it valid under more general circumstances.

Here we propose to rewrite  $B$  (or  $\beta$ ) under the acoustic phonon scattering assumption (we will later discuss how this assumption is valid in different thermoelectric materials), which we call the quality factor since  $B$  is the combination of material properties of a semiconductor that directly relates to the maximum material performance,  $zT$ , when the carrier concentration is optimized.

For materials with conduction from a single spherical Fermi surface, the mobility at the classical limit, when dominated by acoustic phonon scattering can be written as:

$$\mu_{cl} = \frac{(8\pi)^{1/2} \hbar^4 e C_l}{3m^{*5/2} (k_B T)^{3/2} \Xi^2} \quad (1.4)$$

And hence quality factor  $B$  is defined as:

$$B = \left( \frac{k_B}{e} \right)^2 \frac{2e(k_B T)^{3/2} \mu_0 m^{*3/2}}{(2\pi)^{3/2} \hbar^3 \kappa_L} T = \frac{2k_B^2 \hbar}{3\pi} \frac{C_{11}}{m^* \Xi^2 \kappa_L} T \quad (1.5)$$

Here  $C_{11}$  is the longitudinal elastic constant, and  $\Xi$  is the deformation potential. Equation (1.5) reveals that a small effective mass  $m^*$ , small deformation potential  $\Xi$ , together with small lattice thermal conductivity  $\kappa_L$  as favorable features for good thermoelectric materials.

The importance of reducing lattice thermal conductivity,  $\kappa_L$  has been widely accepted and employed in research and will not be further discussed here. In the following sections we will discuss the influence of the other parameters and what is preferred for best thermoelectric performance.

## 1.2 Effective Mass

In the simple case of a single, parabolic and isotropic band, the Fermi surfaces are spherical and the second derivatives of electron energy with respect to its wave vector, which by a common definition is the effective mass  $m^*$ , is a constant scalar. The conduction band of most III–V compounds follows this feature. In many other semiconductors the extremes of bands are off the center of Brillouin Zone and the band structure in this case is referred to as being composed of degenerate valleys,

the number of which is called valley degeneracy  $N_v$ . This aroused the necessity of distinguishing the (density of state) effective mass of a single valley  $m_b^*$  from the total density of state (DOS) effective mass  $m_d^*$ . They are defined so that the carrier density:

$$n = \frac{(2m_d^*k_B T)^{3/2}}{2\pi^2\hbar^3} F_{1/2}(\zeta) \quad (1.6)$$

where

$$m_d^* = N_v^{2/3} m_b^* \quad (1.7)$$

In most multi-valley structures each valley, or carrier pocket in the view of Fermi surfaces, is not spherical. The effective mass is thus a tensor  $m_{ij}^* = \frac{1}{\hbar^2} \left( \frac{d^2\varepsilon}{dk_i dk_j} \right)^{-1}$ . To the first order these valleys are often approximated as ellipsoids, and effective masses along two principle directions are used. In semiconductors like silicon, germanium, and lead chalcogenides they are defined as transverse and longitudinal components  $m_1^* = m_2^* = m_\perp^*$ ,  $m_3^* = m_\parallel^*$ . The DOS effective mass of a single valley is thus averaged as

$$m_b^* = (m_\perp^{*2} m_\parallel^*)^{1/3} \quad (1.8)$$

meanwhile, a different average is defined and called inertial effective mass by Herring [8] and Goldsmid [2]:

$$m_I^* = 3 \left( \frac{2}{m_\perp^*} + \frac{1}{m_\parallel^*} \right)^{-1} \quad (1.9)$$

$m_I^*$  is also referred to as the conductivity effective mass or susceptibility effective mass [9].

Equation (1.4) for multi-valley systems now becomes:

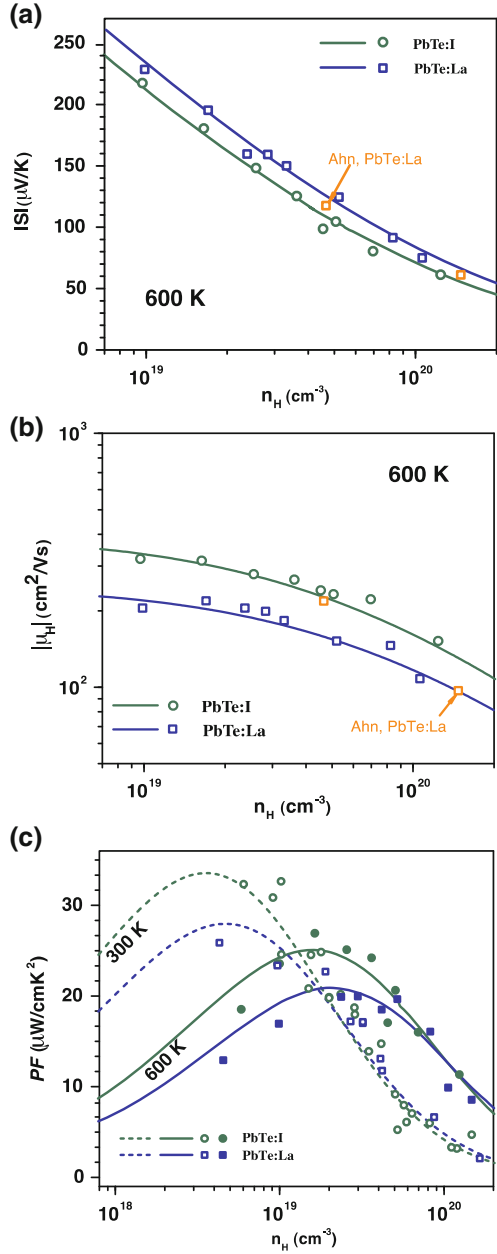
$$\mu_{cl} = \frac{2^{3/2} \pi^{1/2} \hbar^4 e C_l}{3 m_I^* (m_b^* k_B T)^{3/2} \Xi^2} \quad (1.10)$$

$C_{11}$  in Eq. (1.4) is replaced with average longitudinal elastic modulus  $C_l$ , which is a combination of elastic moduli depending on the lattice structure and position of carrier pockets [10]. The quality factor  $B$  now becomes:

$$B = \frac{2k_B^2 \hbar}{3\pi} \frac{C/N_v}{m_I^* \Xi^2 \kappa_L} T \quad (1.11)$$

A large  $m_d^*$ , which usually leads to large Seebeck coefficients and hence apparently is preferred for thermoelectrics, can rise from large effective mass of each valley  $m_b^*$ , or from the large number  $N_v$  of degenerate valleys with small  $m_b^*$ . Since large  $m_b^*$  also means large  $m_I^*$ , the first scenario actually leads to smaller  $B$  and lower  $zT$ , whereas the second scenario (large  $N_v$ ) truly increases  $B$  and  $zT$ .

**Fig. 1.4** **a** Seebeck coefficient as a function of carrier density for La and I doped PbTe, where heavier  $m_b^*$  in La doped samples leads to higher  $S$  values. **b** Mobility as a function of carrier density for La and I doped PbTe, where heavier  $m_b^*$  in La doped samples also leads to lower mobility. **c** The net effect is a lower power factor in La doped samples compared with I doped PbTe



A good demonstration [7] of this has been made in n type PbTe system by using different dopants La and I. The sample doped with La tends to have a higher Seebeck coefficient for the same Hall carrier concentration as I doped sample (Fig. 1.4a), which can be traced to the larger effective mass  $m_b^*$  with La doping, as is also

suggested by theoretical calculation [11]. However, the La doped samples have reduced Hall mobilities (Fig. 1.4b) compared to the I doped samples, which again can be fully explained by the larger  $m_b^*$ . In the end the net effect is a lower  $zT$  in La doped samples (Fig. 1.4c).

The larger effective mass  $m_b^*$  can also partially explain why n type PbS has lower  $zT$  than PbSe. PbS is known to have a larger  $m_b^*$ , at 800 K, it is  $0.23 m_e$  compared with  $0.15 m_e$  for PbSe. The deformation potential coefficient  $\Xi$  is found at 800 K around 28 eV for both compounds. This means the lower mobility in PbS can largely be attributed to the larger  $m_b^*$ , which accounts for an important reason for inferior thermoelectric performance of PbS (Fig. 1.5).

Good thermoelectric materials such as  $\text{Bi}_2\text{Te}_3$ , lead chalcogenides, SiGe and BiSb, have small single-valley effective mass  $m_b^*$ . The total DOS effective mass  $m_d^*$  tend to be larger due to their multi-valley feature. At the same time there are several other systems such as  $\text{CoSb}_3$ ,  $\text{Yb}_{14}\text{MnSb}_{11}$ , and Half Heusler  $\text{ZrNiSn}$  compound, which have very large  $m_d^* > 2 m_e$  as suggested by reported results, and the  $zT$  values are still very promising. Although further studies may reveal that the single-valley effective mass  $m_b^*$  are not as large as indicated by their  $m_d^*$ , this implies that the effective masses, especially  $m_d^*$  alone, is in general not enough as a indicator of good thermoelectric materials.

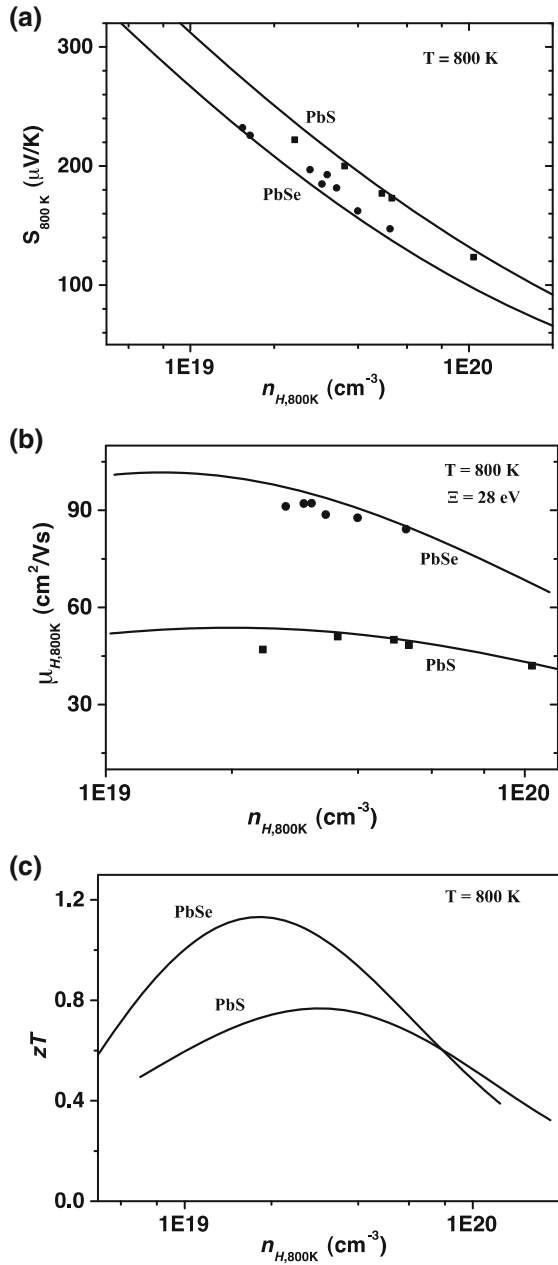
### 1.3 Band Anisotropy/Shape of Carrier Pockets

The effective mass along different directions  $m_{\perp}^*$  and  $m_{\parallel}^*$  can be different in the same valley (band extremum), which is characterized by the band anisotropy factor  $K = m_{\parallel}^* / m_{\perp}^*$ . Unless with additional evidence to the contrary, the carrier scattering rate in such bands are considered isotropic and the difference in relaxation time is solely due to the difference in effective mass. Thus, as long as the macroscopic properties are isotropic the quality factor  $B$  discussed above, which is isotropic in nature, is still valid.

If a spherical electron pocket is distorted and elongated in one direction while the density of state effective mass stays the same, the direction with smaller effective mass would contribute to conduction more greatly than the directions with heavier masses. The conduction effective mass  $m_l^*$  is thus different even though  $m_d^*$  is the same. When the (drift) mobility is plotted against carrier density for different  $K = m_{\parallel}^* / m_{\perp}^*$  higher mobilities are found when  $K$  differs from 1 (Fig. 1.6), which leads to increased power factor and  $zT$  since  $m_d^*$  and hence  $S$  is unchanged. The electron pockets in PbTe are more anisotropic than in PbSe while the  $m_d^*$  are very close to each other, this helps n type PbTe to achieve a higher mobility and  $zT$  compared to PbSe.

$K$  also has its influence on the Hall factor  $A(K, \zeta)$  which relates the Hall mobility  $\mu_H$  with the drift mobility  $\mu$  through  $\mu_H = A\mu$ . Such influence is on the order of 10% when  $K$  is increased to 5 or decreased to 0.2 from 1. When taking this into account, the directly observed relationship between Hall mobility  $\mu_H$  and Hall

**Fig. 1.5** **a** Seebeck coefficient as a function of carrier density in PbSe and PbS at 800 K. **b** Mobility as a function of carrier density in PbSe and PbS at 800 K, the difference is mainly due to the larger  $m_b^*$  in PbS. **c**  $zT$  as a function of carrier density at 800 K, which is partly due to the larger  $m_b^*$  in PbS, the other reason being the higher lattice thermal conductivity



carrier density  $n_H$  from Hall measurement has a distorted and different appearance (Fig. 1.7). Since  $m_I^*$ , through mobility  $\mu$ , influences the thermoelectric quality factor, it can be drawn from Fig. 1.6 that distorted electron pockets ( $K \neq 1$ ) would have better thermoelectric transport properties than spherical ones given the same density

**Fig. 1.6** Drift mobility as a function of carrier density assuming the same density of state effective mass  $m_b^*$  but different band anisotropy. All parameters used in the calculation are taken from n type PbSe. Distorted electron pockets have higher mobility compared with spherical ones

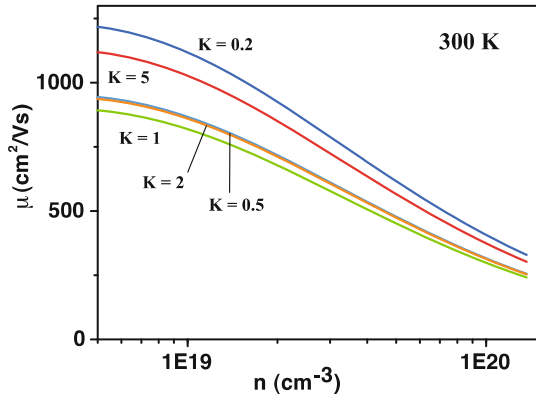
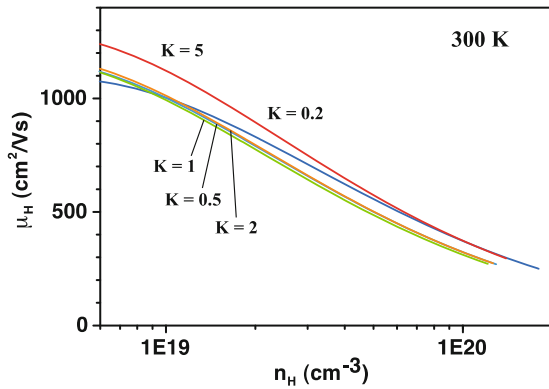


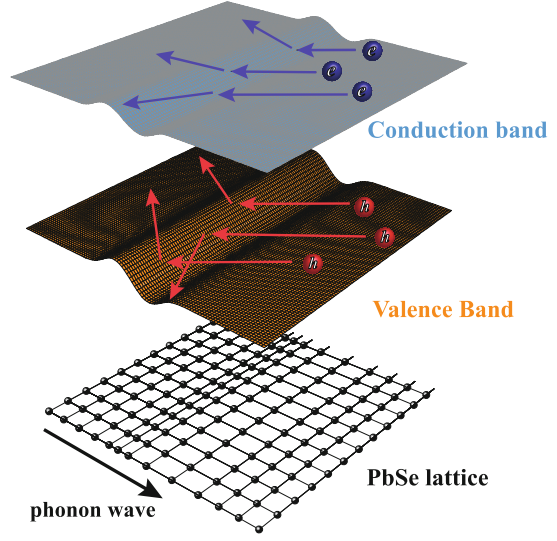
**Fig. 1.7** The result of Fig. 1.6, when plotted with directly observed Hall mobility and Hall carrier density, are distorted and seem to have “different” dependence of  $K$



of state effective mass. More fundamentally this can be regarded as another specific case of smaller conduction effective mass being more favorable for thermoelectrics.

In some semiconductor systems  $m_b^*$  is temperature dependent. For example in lead chalcogenides, the following relation is found  $d \ln m_b^* / d \ln T = 0.4 - 0.5$ . How  $K$  would change with  $m_b^*$  is not well understood yet. The k·p perturbation theory suggests both longitudinal and transverse components of  $m_b^*$  are affected by the interaction between the conduction and valence band and thus should be temperature dependent [9]. But to our knowledge no conclusion has been made that they would change in the same manner. Still to the first order, it should be a good approximation by using constant  $K$  from calculation or low temperature data and keeping in mind that such approximation might not be as accurate at high temperature.

**Fig. 1.8** Schematic carrier-phonon interaction via deformation potential scattering. Lattice was deformed by phonon waves, which produce the potential energy fluctuation in each band, resulting in scattering of carriers. In PbSe such fluctuation is smaller in the conduction band than that in the valence band, the electron mobility is thus higher than that of holes



## 1.4 Deformation Potential Coefficient

As an acoustic phonon wave propagates through a crystal it causes compression and dilation of the local lattice which introduces a perturbation of the potential energy of bands and hence the scattering of carriers. Such a process is called the deformation potential scattering from acoustic phonons, or more commonly, acoustic phonon scattering in short (Fig. 1.8). The concept of “deformation potential” was first used by Bardeen and Shockley [12] and can be regarded as a measure of the strength of carrier-phonon interaction and is therefore sometimes referred to as the electron-phonon coupling constant [13, 14].

The relaxation time of acoustic phonon scattering can be written as [9, 12]:

$$\tau_{ac} = \frac{\hbar C_{11} N_V}{\pi k_B T \Xi^2} g(\varepsilon)^{-1} f(\varepsilon) \quad (1.12)$$

Where  $\varepsilon = E/k_B T$  is the reduced energy of carriers,  $g(\varepsilon)$  is the density of states,  $\Xi$  is the deformation potential, and the form of  $f(\varepsilon)$  depends on the band model. In the simplest case with a single extreme at the center of the Brillouin Zone, and using the single parabolic band model:

$$\tau_{ac} = \frac{\pi \hbar^4 C_{11}}{2^{1/2} m^{*3/2} (k_B T)^{3/2} \Xi^2} \varepsilon^{-1/2} \quad (1.13)$$

so that the drift mobility for arbitrary chemical potential is given by:

$$\mu = \frac{2^{1/2} \pi \hbar^4 e C_{11}}{3 m^{*5/2} (k_B T)^{3/2} \Xi^2} \frac{F_0(\eta)}{F_{1/2}(\eta)} \quad (1.14)$$

$\eta = \zeta/k_B T$  is the reduced chemical potential,  $F_\lambda(\eta)$  are the Fermi integrals:

$$F_\lambda(\eta) = \int_0^\infty \frac{\varepsilon^\lambda}{1 + \text{Exp}(\varepsilon - \eta)} d\varepsilon \quad (1.15)$$

In multi-valley semiconductors, the longitudinal elastic constant  $C_{11}$  is replaced by the average longitudinal elastic constant [10, 15]  $C_l$ , the single effective mass is replaced by an inertial effective mass  $m_l^*$  and a DOS effective mass of a single valley  $m_b^*$ .  $\Xi$  (called here the deformation potential coefficient) is a combination of two deformation potential components  $\Xi_d$ ,  $\Xi_u$  defined by energy shifts caused by different strain elements (for details about the definition see ref. [9, 10, 16, 17]). For small gap systems, a nonparabolic Kane band model is usually more accurate than the single parabolic band model. In lead chalcogenides the Kane model has even been developed to take into account the energy dependence of interaction matrix. Thus Eqs. (1.13) and (1.14) above are replaced by:

$$\tau_{ac} = \frac{\pi \hbar^4 C_l}{2^{1/2} m_b^{*3/2} (k_B T)^{3/2} \Xi^2} (\varepsilon + \varepsilon^2 \alpha)^{-1/2} (1 + 2\varepsilon \alpha)^{-1} \left[ 1 - \frac{8\alpha(\varepsilon + \varepsilon^2 \alpha)}{3(1 + 2\varepsilon \alpha)^2} \right]^{-1} \quad (1.16)$$

$$\mu = \frac{2\pi \hbar^4 e C_l}{m_l^* (2 m_b^* k_B T)^{3/2} \Xi^2} \frac{{}_3F_{-2}^1}{{}_0F_0^{3/2}} \quad (1.17)$$

here  $\alpha = k_B T / \Delta E$ ,  $\Delta E$  is the gap between the interacting conduction and valence band. The generalized Fermi integral is defined as:

$${}_n F_l^m(\eta) = \int_0^\infty \left( -\frac{\partial f}{\partial \varepsilon} \right) \varepsilon^n (\varepsilon + \varepsilon^2 \alpha)^m [(1 + 2\varepsilon \alpha)^2 + 2]^{1/2} d\varepsilon \quad (1.18)$$

In either model the deformation potential coefficient  $\Xi$  significantly influences mobility as this term is squared. A smaller  $\Xi$  is always desirable for thermoelectrics.

In PbTe and PbSe, the conduction band and the valence band at the L point have almost identical effective mass, but the conduction band is found to have a smaller deformation potential coefficient  $\Xi$  than the (light) valence band. smaller  $\Xi$  gives these n type lead chalcogenides similarly high  $zT$  [18] as the p type doped materials, where the presence of a highly degenerate secondary valence band plays an essential role for their good thermoelectric properties.

Despite its importance to thermoelectrics, little is known or studied by researchers in this field about the deformation potential coefficient. Data are only available for a few thermoelectric semiconductors that have broader interests for other fields also. Evaluating the deformation potential for each band of a compound is also very difficult and large discrepancy exists in the experimental result for  $\Xi_d$  and  $\Xi_u$ , which add another factor to the difficulty of comparing  $\Xi$  from mobility data with those from other measurements.

In principle  $\Xi$  can be obtained by calculating the quantum mechanic electron-phonon interaction matrix. Such calculation was developed and explained by Bir and Pikus [19, 20].

The deformation potential component  $\Xi_u$  can also be obtained from the piezoresistance tensors of intrinsic samples [9, 10]. Consistency is poor among reports from different groups. For n type Ge and Si,  $\Xi_u$  is found to be between 16–19 eV, and 7–10 eV, respectively [10, 17, 21]. For PbTe this number is between 2 and 4 eV for the conduction band and 4–8 eV for the valence band [9, 16]. Based on the available literature to us there is no reliable experimental result on  $\Xi_d$ . For lead chalcogenides there is even discrepancy on whether the value is larger (from mobility data) or smaller (from calculation) than the magnitude of  $\Xi_u$ .

The deformation potential under hydrostatic pressure ( $3\Xi_d + \Xi_u$ ), especially the difference between the conduction and valence band, is more commonly estimated. This is usually called the optical isotropic deformation potential  $D_{iso} = (3\Xi_d + \Xi_u)_c - (3\Xi_d + \Xi_u)_v$ .

For example Bardeen and Shockley [12] suggested several methods to determine  $D_{iso}$  of Si and Ge based on the change of band gap with temperature or pressure. Ferreira [16] compared  $D_{iso}$  of PbTe estimated from the temperature and pressure dependence of the band gap with that determined from APW calculation.  $D_{iso}$  varies only between 10 and 15 eV among these methods. Zasavitskii obtained a similar result of 10 eV from magneto-optical absorption data [22]. In his work  $D_{iso}$  for PbSe was also determined to be 14 eV, while Wu's optical spectroscopy result [23] on quantum well structure of PbSe was 17 eV (more comparison is given by Zasavitskii in his paper). But still, these numbers are quite different from the results we get from the mobility of n type and p type PbSe ( $\sim 10$  eV) and PbTe ( $\sim 5$  eV).

Besides the difficulty in measurements, another factor contributing to the poor consistency between deformation potential values from mobility data and other methods lies in the basic assumption that acoustic phonon scattering is the only (predominant) carrier scattering mechanism. In the following section we provide a detailed discussion about why, in most cases, this assumption is qualitatively valid and how it is adjusted in systems where other similar scattering mechanisms also exist.

Our conclusion from the following discussion in Sects. 1.5 and 1.7 is that the best way to determine the deformation potential coefficient  $\Xi$  in the expression of quality factor is by fitting the mobility data from several samples with  $n_H$  close to the optimum range. In this way, the result is actually a combined effective value taking into account the most studied deformation potential scattering from acoustic phonons (correspondingly  $\Xi_{ac}$ ), the deformation potential scattering from optical phonons whose magnitude is characterized by  $\Xi_{op}$  [see Eq. (1.23)], and additionally the inter-valley scattering for complex band structures when allowed (see Sect. 1.7).

In the Table 1.1 we list the  $\Xi$  data estimated from mobility for a few systems that are, or can be, approximated as, single band systems with relevant data available. Due to the lack of systematic study some of the values are rough estimation and caution is needed when using these results.

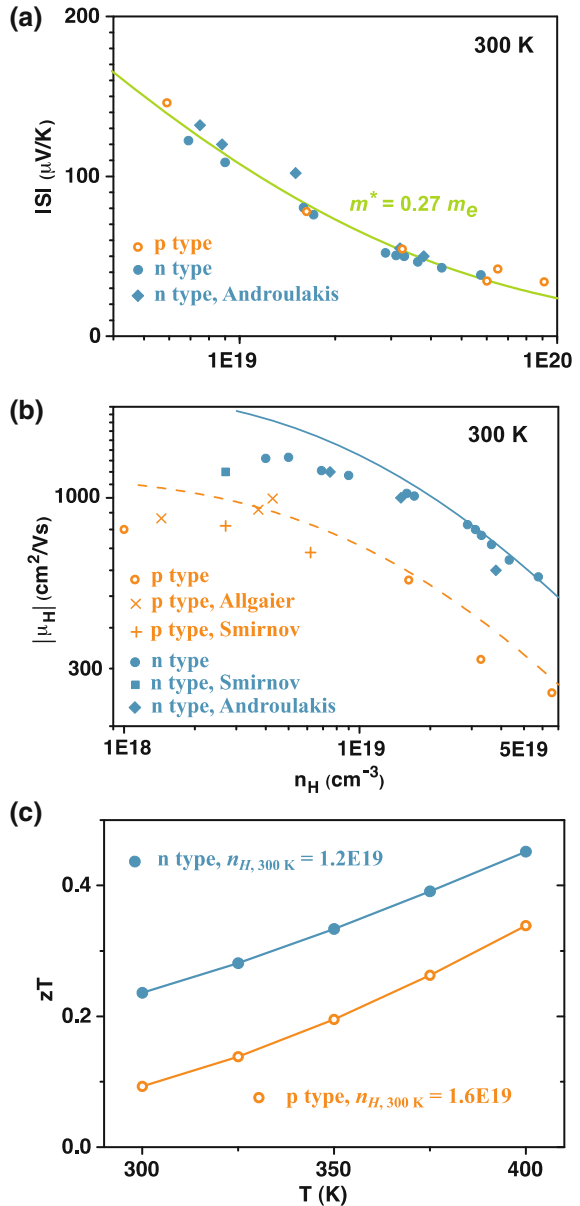
A direct demonstration of different deformation potential  $\Xi$  affecting mobility, and thus  $zT$ , is rare since other parameters might be different at the same time.

**Table 1.1** The deformation potential coefficient, together with other material parameters ( $\Delta X$  the electronegativity difference) for compound semiconductors

	$\mu_0 m_d^{*3/2}$ ( $\text{cm}^2/\text{Vs}$ )	$\Xi$ (eV)	$m_d^*$ ( $m_e$ )	$m_l^*$ ( $m_e$ )	$N_v$	$C_I \times 10^{-10}$ (Pa)	$\Delta X$	Coordination number	Note
PbSe(n)	160	25	0.27	0.1	4	9.1	0.22	6	Modeling results
PbSe(p)	110	35	0.27	0.1	4				
PbTe(n)	200	22	0.26	0.1	4	7.1	0.23	6	
PbTe(p)	100	25	0.26	0.1	4				
PbS(n)	160	27	0.41	0.16	4	11.1	0.25	6	
Diamond (n)	5,370	9	1.84	0.46	6	115.7		4	Ref. [6], consistent with ref [12, 24].
Si(n)	1,700	8	1.1	0.27	6	18		4	
Ge(n)	1,900	10	0.55	0.12	4	16		4	
$Bi_2Te_3$ (n)	400	24	0.9 (0.35/a)		6		0.08	6	Ref. [6]. $m_d^*$ estimated from seebeck data from CRC Handbook, $C_I$ and $m^*$ in basal plane from ref. [24]. Larger $\Xi$ reported in ref. [25]
$Bi_2Te_3$ (p)	600	24	0.8 (0.35/a)		6				
$CoSb_3$ (p)	75	33	0.07	0.07	1	10	0.17		Mobility from ref. [26, 27], $C_I$ use bulk modulus from ref. [28]
$Bi_{0.9}Sb_{0.1}$ (n)	400	18	0.17		3	6.3	0.03	6	$m_d^*$ and mobility from unpublished result, $C_I$ use $C_{11}$ of Bi
$La_3Te_4$ (n)	5	29	0.62	0.39	2	5	1	6 (8)	Ref. [29, 30], $C_I$ use bulk modulus. conduction band is split into 3 bands. $\Xi$ only for qualitative compare ref [6].
$Bi_2Se_3$ (n)	42	20	0.15 (/a)		1		0.53	6	Ref. 1. $\Xi$ from ref. [24, 31]. polar scattering is believed, important in III-V and II-VI compounds, $\Xi$ might be greatly overestimated here and after
InSb(n)	95	33	0.011		1	8.2	0.27	4	$C_I, \Xi$ from ref. [24]
InP (n)	114	21	0.077		1	12	0.41	4	Ref. [6] Values for GaAs and GaN consistent with ref. [24]. Secondary band minimum close to band edge
GaSb(n)	50	>30	0.04		1	10.4	0.24	4	
GaAs(n)	160	20	0.067		1	14.1	0.37	4	
GaN	31	25	0.2		1	36.3	1.23	4	
ZnSe(n)	38	18	0.16		1	10.7	0.9	4	
CdTe(n)	30	25	0.09		1	7	0.41	4	

Values are for 300 K

**Fig. 1.9** **a** Seebeck coefficient as a function of carrier density for n-type and p-type PbSe, the same effective mass is indicated by the same  $S-n_H$  dependence. **b** Mobility as a function of carrier density in n-type and p-type PbSe, mobility in n-type PbSe is higher due to a smaller deformation potential coefficient  $\Xi$ . **c**  $zT$  in n type PbSe is found higher than in p type as a result of smaller  $\Xi$



However, such an example [18] can be found between the n-type and p-type PbSe. The second maxima of the valence band in PbSe is deep enough ( $\sim 0.3$  eV) so that for a wide range of carrier concentrations both the n- and p-type samples can be regarded as having a single (degenerate) band (the L band). The conduction band and valence

band are almost identical: the DOS effective mass  $m_d^*$  is the same as supported by the single Pisarenko ( $S$  vs  $n_H$ ) relation observed for both n- and p-type samples (Fig. 1.9). The shape of the carrier pockets ( $K$  value) is also the same as revealed by cyclotron resonance [9]. The speed of sound, representing the elastic properties, is also found independent of dopant type. Thus the observed difference in mobility can only be due to different deformation potential coefficients  $\Xi$ , which can also be concluded from the direct measurement of  $D_{iso}$  discussed above. As a result, n-type PbSe shows higher  $zT$  than the p-type material having the same carrier concentration.

## 1.5 Carrier Scattering from Optical Phonons

Mobility in semiconductors is partially determined by scattering between carriers and various scattering centers. The magnitude of each scattering mechanism is usually both energy and temperature dependent. Even though the mobility (or the relaxation time) is, strictly speaking, a combined contribution from all mechanisms there are only a few, if not one, of them that dominate the total relaxation time within a certain temperature and carrier concentration range.

Scattering by impurities (both neutral and ionized), dislocations and boundaries are weak in magnitude and do not increase with temperature. They are therefore usually noticeable only at low temperatures. For thermoelectrics the behavior of heavily doped bulk semiconductors around or above room temperature is of most interest, where the interaction between electrons and phonons is of the most importance.

Besides the most stressed and studied acoustic phonon scattering, in systems with more than one atom per unit cell there are also optical phonons. And for complex structures, where many good thermoelectric materials are found, optical phonon branches are prevalent. Optical phonons interact with charge carriers in two ways: one is the deformation potential scattering from optical phonons that is analogous to that of acoustic phonons, the other is the polar scattering seen in polar semiconductors which is from the electrostatic force due to the opposite phase of oscillation between the neighboring differently charged lattice ions.

### 1.5.1 Deformation Potential Scattering from Optical Phonons

Electron-phonon interaction involving optical phonons is generally inelastic due to their high energy. This means the basic assumption of relaxation time approximation used to derive expressions for transport parameters from the Boltzmann transport equation is not valid [3, 17, 32] and there will not strictly be a universal expression for  $\tau$ . Nevertheless, a relaxation time  $\tau$  so defined, is however approximated given that certain requirements are met [9, 17, 33].

For the deformation potential scattering by optical phonons, Seeger [17] gives a clear derivation and his expression (which Askerov [32] called the nondegenerate form) for momentum relaxation time  $\tau_{odp}$  for a single parabolic, and isotropic band is:

$$\begin{aligned} \tau_{odp} = & \frac{2^{1/2}\pi\rho\hbar^2k_B\Theta}{m^{*3/2}(k_B T)^{1/2}\Xi_{op}^2} \\ & \times [\exp(\Theta/T) - 1][(\varepsilon + \Theta/T)^{1/2} + \exp(\Theta/T)\text{Re}\{(\varepsilon - \Theta/T)^{1/2}\}]^{-1} \end{aligned} \quad (1.19)$$

where  $\rho$ ,  $\Theta$ , and  $\Xi_{op}$  are the density, optical phonon Debye temperature and deformation potential for optical phonon scattering (in unit of  $eV/cm$ ), respectively. the terms  $(\varepsilon + \Theta/T)^{1/2}$  and  $(\varepsilon - \Theta/T)^{1/2}$  represent the absorption and emission of a optical phonon, respectively, and the real part of the latter one is taken since emitting a phonon with energy higher than the electron is prohibited. A similar form of the same equation is also used by Chin et al. [34]. From Eq. (1.19) when  $\Theta/T \ll 1$  one get:

$$\tau_{odp} \propto m^{*-3/2}T^{-3/2}\varepsilon^{-1/2} \quad (1.20)$$

This is exactly the same dependence found for acoustic phonon scattering (Eq. 1.16, see Fig. 6.14 in ref. [17]).

For degenerate semiconductors another form of  $\tau_{odp}$  is used [32, 35]. In the Kane band model with energy dependent interaction matrix:

$$\begin{aligned} \tau_{odp} = & \frac{2\hbar^2 a^2 \rho (k_B \Theta)^2}{\pi (2m_b^* k_B T)^{3/2} \Xi_{op}^2} (\varepsilon + \alpha \varepsilon^2)^{-1/2} (1 + 2\alpha \varepsilon)^{-1} \\ & \times \left[ \left( 1 - \frac{\alpha \varepsilon (1 - K_m)}{1 + 2\alpha \varepsilon} \right)^2 - \frac{8\alpha (\varepsilon + \alpha \varepsilon^2) K_m}{3(1 + 2\alpha \varepsilon)^2} \right]^{-1} \end{aligned} \quad (1.21)$$

This equation is lengthy because it accounts for very detailed knowledge about lead chalcogenides' band structure ( $K_m = \Xi_{op}^v / \Xi_{op}^c$  for electrons, or  $\Xi_{op}^c / \Xi_{op}^v$  for holes) together with the Kane model. In general the last term can be neglected without altering the final result much. Equation (1.21) (the unit of  $\Xi_{op}$  is in eV) can be transformed into a form analogous to that for  $\tau_{ac}$  with the same level of detail only by replacing  $\Xi$  with  $\Xi_{op}(\frac{\pi\hbar}{ak_B\Theta})(\frac{C_L}{\rho})^{1/2}$ , See Eq. (1.23).

A third version of  $\tau_{odp}$  (for lead chalcogenides) is given by Morgovskii and Ravich [36]:

$$\tau_{odp} = \frac{\pi M \hbar^4 \omega_l^2}{(2m_b^* k_B T)^{3/2} \Omega C^2} (\varepsilon + \alpha \varepsilon^2)^{-1/2} (1 + 2\varepsilon\alpha)^{-1} \left[ \frac{\alpha \varepsilon (1 + \alpha \varepsilon)}{(1 + 2\varepsilon\alpha)^2} \right]^{-1} \quad (1.22)$$

where  $M/\Omega$ ,  $\omega_l$ ,  $C$  are the atomic mass/volume of a unit cell, the frequency of longitudinal optical phonons (assuming constant) and an interaction constant equivalent to deformation potential (in unit of  $eV/m$ ), respectively. Again, this equation shares all the key terms with Eq. (1.16) (consider the last term in each as a minor correction).

There are few reports on the value of deformation potential for optical phonons. For n type Ge Jacoboni [37] suggested this value to be  $5.5 \times 10^8$  eV/cm, which is equivalent to 3.3 eV when rewriting Eq. (1.19) in a analogous form of Eq. (1.16),

comparing with about 10 eV for  $\Xi_{ac}$  from acoustic phonon scattering in this material. Deformation potential scattering from optical phonons is negligible in n type Si [38]. For III–V compounds Takeda [39] gives  $\Xi_{op}$  around  $1.4 \times 10^{10}$  eV/cm for GaAs and InP, which is considerably larger than the value in n type Ge.

Wiley [40, 41] and Costato [42] have formulated  $\Xi_{op}$  in terms of material parameters and compared the calculated results with p-type IV or III–V semiconductors. However, in these materials the conduction behavior has multiple-band character, making the reported results phenomenological instead of reflecting the nature of electron-phonon interaction in a given band.

Using an effective deformation potential coefficient  $\Xi_{eff}$  in Eq. (1.16), the influence of deformation potential from optical phonons is inherently considered (Eq. 1.23).

$$\begin{aligned}
 \tau_{eff}^{-1} &= \tau_{ac,0}^{-1} \tau_{\varepsilon}^{-1}(\varepsilon) \text{(Eq.1.6)} + \tau_{odp,0}^{-1} \tau_{\varepsilon}^{-1}(\varepsilon) \text{(Eq.1.21)} \\
 &= \frac{2^{1/2} (m_b^* k_B T)^{3/2} \Xi_{ac}^2}{\pi \hbar^4 C_l} \tau_{\varepsilon}^{-1}(\varepsilon) + \frac{2^{1/2} \pi (m_b^* k_B T)^{3/2} \Xi_{op}^2}{\hbar^2 \alpha^2 \rho (k_B \Theta)^2} \tau_{\varepsilon}^{-1}(\varepsilon) \quad (1.23) \\
 &= \frac{2^{1/2} (m_b^* k_B T)^{3/2}}{\pi \hbar^4 C_l} \left( \Xi_{ac}^2 + \Xi_{op}^2 \left( \frac{\pi^2 \hbar^2 C_l}{\alpha^2 \rho (k_B \Theta)^2} \right) \right) \tau_{\varepsilon}^{-1}(\varepsilon) \\
 &= \frac{2^{1/2} (m_b^* k_B T)^{3/2} \Xi_{eff}^2}{\pi \hbar^4 C_l} \tau_{\varepsilon}^{-1}(\varepsilon), \quad \Xi_{eff} = \left[ \Xi_{ac}^2 + \Xi_{op}^2 \left( \frac{\pi^2 \hbar^2 C_l}{\alpha^2 \rho (k_B \Theta)^2} \right) \right]^{1/2}
 \end{aligned}$$

### 1.5.2 Polar Scattering from Optical Phonons

If the lattice contains more than one species of atoms, carriers can also be scattered by the changing polarity due to optical vibration. There are two important quantities for polar optical scattering. The first is the dimensionless polar coupling constant  $\alpha_{po}$ , which governs the magnitude of interaction between carriers and polarization of optical phonons [17, 43, 44]:

$$\alpha_{po} = \frac{e^2}{4\pi \hbar} \left( \frac{m^*}{2\hbar\omega_l} \right)^{1/2} (\varepsilon_{\infty}^{-1} - \varepsilon_0^{-1}) \text{(SI units)} \quad (1.24)$$

where  $\varepsilon_0$ ,  $\varepsilon_{\infty}$  are the static and high frequency dielectric constant (with unit F/m, not relative values).

The second is the optical phonon temperature  $k_B \Theta = \hbar\omega_l$  (close to the Debye temperature).

For general cases  $\tau$  can not be defined due to the inelastic nature of the polar scattering, and the transport parameters are calculated using numerical methods. Detailed calculations have been done by researchers such as Howarth and Sondheimer [33], and Ehrenreich [45]. In III–V [34, 39, 46] and II–VI [47, 48] semiconductors due to their high  $\Theta$  and the major interest in lightly doped samples, the polar scattering by

optical phonons is considered important and such calculations and results are widely used.

For most good thermoelectric materials with potential application in energy recovery, when  $T > \Theta$ , which is usually the temperature range of most interest, a relaxation time can be defined. Since these materials are heavily doped, the screening of polarity vibration by free electrons must also be considered. Ravich's derivation [9, 43, 49] takes into account this together with the band nonparabolicity in lead chalcogenides, which gives (all parameters in SI units):

$$\tau_{po} = \frac{4\pi\hbar^2\varepsilon^{1/2}}{2^{1/2}(k_B T)^{1/2}e^2 m_b^{*1/2}(\varepsilon_\infty^{-1} - \varepsilon_0^{-1})} (1 + 2\varepsilon\alpha)^{-1} (1 + \varepsilon\alpha)^{1/2} \left\{ \left[ 1 - \delta \ln \left( 1 + \frac{1}{\delta} \right) \right] - \frac{2\alpha\varepsilon(1 + \varepsilon\alpha)}{(1 + 2\varepsilon\alpha)^2} \left[ 1 - 2\delta + 2\delta^2 \ln \left( 1 + \frac{1}{\delta} \right) \right] \right\}^{-1} \quad (1.25)$$

$$\delta(\varepsilon) = \frac{e^2 m_b^{*1/2} N_V}{2^{1/2} \varepsilon (k_B T)^{1/2} \pi \hbar \varepsilon_\infty} (1 + \varepsilon\alpha)^{-10} F_1^{1/2} \quad (1.26)$$

Each parameter in the expression of  $\tau_{po}$  can be determined from direct measurements.

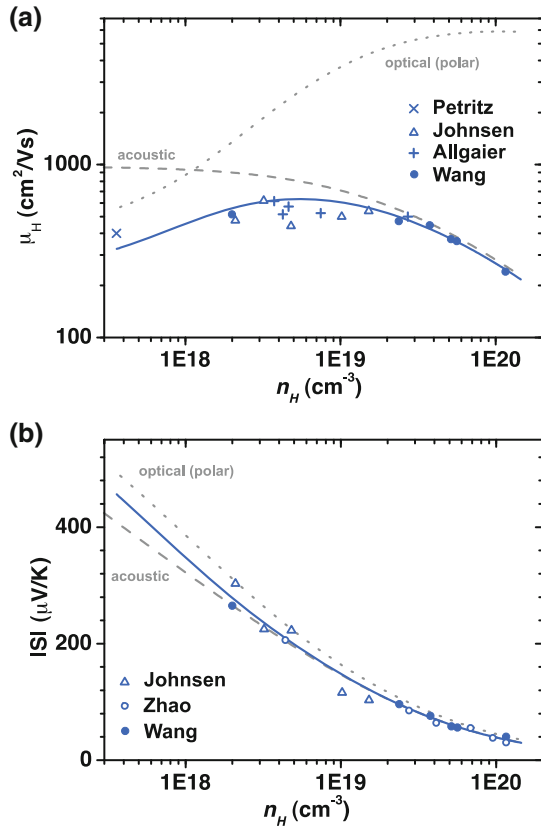
Equation (1.25) has been used by other researchers when studying the scattering mechanism in PbTe [35, 50, 51] and Bi<sub>2</sub>Te<sub>3</sub> [25]. It should also be a reasonable expression for such scattering mechanism in other systems with Kane band behavior, such as CoSb<sub>3</sub> at high temperature ( $\Theta$  for CoSb<sub>3</sub> is  $\sim 300$  K). Qualitatively from Eq. (1.25):

$$\tau_{po} \propto m^{*-1/2} T^{-1/2} \varepsilon^{1/2} \quad (1.27)$$

Compared to Eq. (1.16) for acoustic phonon scattering, relaxation time governed by polar scattering from optical phonons has a weaker dependence on temperature and effective mass [ $-1/2$  for each compared to  $-3/2$  in Eq. (1.16)]. It will increase, instead of decrease as for the case of acoustic phonon scattering, with carrier energy  $\varepsilon$ . This implies it would be less important for most thermoelectric materials above room temperature. In more general case, the exponent  $r$  in  $\tau_{po} \propto \varepsilon^r$  is plotted against  $\Theta/T$  by Ehrenreich [17, 45],  $r$  changes greatly with  $T$  and there is a singularity around  $T = \Theta/2$ .

For PbS the calculated mobility governed by the acoustic phonon scattering and polar scattering from optical phonons is plotted in Fig. 1.10. Data shown in Fig. 1.10 are taken from results reported by Petritz [52], Johnsen [53], Allgaier [54], Zhao [55] and Wang [56]. The polar scattering is found to be important when the carrier density is below  $10^{19} \text{ cm}^{-3}$ . In fact, polar scattering is responsible for the deviation of measured mobility from that calculated under the acoustic phonon scattering assumption at low carrier densities. It can be also seen that if the mobility of purest PbS is taken as  $\mu_0$  to evaluate B the quality factor of PbS would be greatly underestimated at 300 K (the calculated mobility value at classical limit under acoustic phonon scattering assumption should be used). While leading to lower mobilities,

**Fig. 1.10 a** Mobility and **b** Seebeck coefficient of PbS at 300 K as a function of carrier density. *Curves* are calculated results from acoustic phonon scattering (*dashed*), polar scattering (*dotted*) and the two combined (*solid*)



the polar scattering would also result in higher Seebeck coefficient in the low doping region. As the carrier density increases, the influence from polar scattering decreases and at 300 K when the carrier density is above 10<sup>19</sup> cm<sup>-3</sup> the polar scattering can be neglected and acoustic phonon scattering becomes predominant. Moreover the polar scattering has a weaker temperature dependence, which means that the carrier density at which acoustic phonon scattering becomes predominant would further decrease as the temperature increase.

Lead chalcogenides are unique compounds in term of their extraordinarily large static dielectric constants. For instance for PbTe,  $\epsilon_0$  around 400 has been reported by different groups from different measurement techniques [57, 58]. In contrast,  $\epsilon_0$  for most III-V and II-V compounds [24] are usually from 10 to 20. Considering the low Debye temperatures in lead chalcogenides, large polar coupling constants  $\alpha_{po}$  would be expected in these compounds (Eq. 1.24). In the table below  $\alpha_{po}$  is compared for a few semiconductors (data from the Landolt-Börnstein Database unless otherwise cited). Lead chalcogenides are seen to have larger  $\alpha_{po}$  compared to other typical

**Table 1.2** The polar coupling constant for a few compound semiconductors

	$\epsilon_0$	$\epsilon_\infty$	$\Theta$	$\alpha_{po}$	Comment
PbTe <sup>a</sup>	414	33	160	0.29	$\Theta$ from optical phonon frequency from ref. [9], $m^*$ use 300 K value from Seebeck data
PbSe <sup>a</sup>	204	23	190	0.36	
PbS <sup>a</sup>	169	17	300	0.45	
CoSb <sub>3</sub>	42 cal <sup>b</sup>	32 cal <sup>b</sup>	306 <sup>d</sup>	0.07	For p type, $m^*$ use 0.15 $m_e$
		25 exp <sup>c</sup>			
Bi <sub>2</sub> Te <sub>3</sub>	290 (//c)	85 (//c)	164	0.13 (//c)	$m^*$ from Seebeck data from CRC handbook
	75 (c)	50 (c)		0.07 (c)	
GaAs	13	11	344	0.08	
InSb	17	16	203	0.01	
ZnO <sup>e</sup>	8	4	660	1.02	
CdTe	10	7	158	0.41	

<sup>a</sup>ref. [59], <sup>b</sup>ref. [60], <sup>c</sup>ref. [61], <sup>d</sup>ref. [62], <sup>e</sup>ref. [48]

thermoelectric materials as well as III–V compounds, whereas some II–V compounds show the largest  $\alpha_{po}$ , which stems from their small yet different dielectric constants.

From the result shown in Fig. 1.10 and Table 1.2 the polar scattering is important around room temperature in lightly doped lead chalcogenides. Its magnitude in other compounds would be less as can be judged from the values of  $\alpha_{po}$ . For most heavily doped thermoelectric materials neglecting the contribution of polar scattering from optical phonons should not lead to drastic error in modeling and the acoustic phonon scattering assumption can be considered valid.

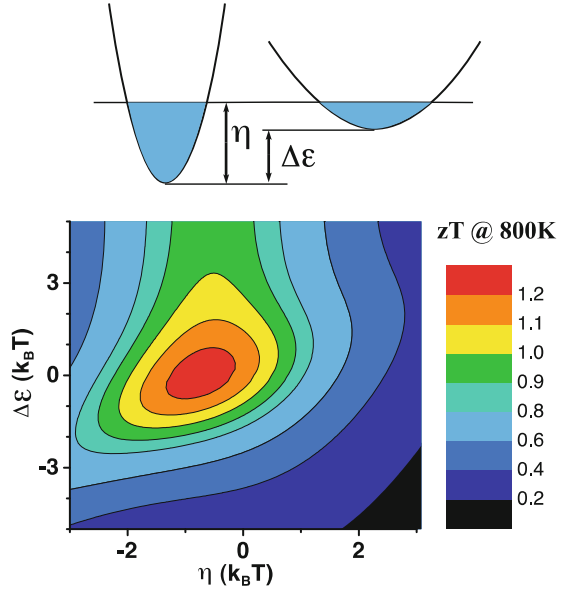
## 1.6 Band/Valley Degeneracy

The band/valley degeneracy  $N_v$ , or, the number of bands/valleys contributing to the carrier transport, is in the numerator of the quality factor  $B$  and therefore larger  $N_v$  is desirable for thermoelectrics.

Considering the Seebeck coefficient  $S$  as only a function of the chemical potential  $\zeta$  ( $S$  is linked to  $m_d^*$  through chemical potential  $\zeta$ ), with a constant  $S$ , a larger  $N_v$  will lead to a larger carrier concentration  $n$ . Since  $\mu$  is not a function of  $N_v$  [When inter-valley scattering is negligible, Eq. (1.16)], the net effect will be an increase in electrical conductivity and  $zT$ .

In Fig. 1.11 the calculated  $zT$  (800 K) of a system with two conduction bands (or analogously, valence bands) is plotted against both  $\eta(= \zeta/k_B T)$  and  $\Delta\epsilon(= \Delta E/k_B T)$ , the reduced energy gap between the two bands). The calculation is based on parabolic, isotropic bands dominated by acoustic phonon scattering. The bipolar conduction and possible inter-band scattering is not considered. Typical parameters found in thermoelectric materials are used for these two bands:  $m^* = 0.2$  and 1,

**Fig. 1.11** Calculated  $zT$  at 800 K in a two-band system as function of chemical potential  $\eta$  and band offset  $\Delta\varepsilon$ . Highest  $zT$  is achieved when the two bands are aligned



$\Xi = 15$ ,  $N_v = 1$ ,  $C_I = 91$  GPa and  $\kappa_L = 0.8$  W/mK. The highest  $zT$  is achieved when  $\Delta\varepsilon = 0$ , i.e., when the two bands are aligned. The band alignment results in an increased effective  $N_v$ .

In fact, most good thermoelectric materials are of multi-valley feature: The conduction band of Si has 6 degenerate valleys and Ge has 4, which is an important reason for their superior electronic properties (and SiGe alloys make good thermoelectric materials when the thermal conductivity is suppressed). In the half-Heusler compound NiTiSn (ZrNiSn) the conduction band [63, 64] has  $N_v = 3$  and the compound when doped n-type has shown good thermoelectric properties [65, 66]. In  $\text{Bi}_2\text{Te}_3$  both the conduction and valence band are of  $N_v = 6$ . For lead chalcogenides,  $N_v = 4$  for the conduction band and the primary valence band, additionally there is a secondary valence band with  $N_v = 12$  making the effective  $N_v$  exceptionally large. In some other systems, this multi-valley feature manifests as additional bands separated from the primary band edge by a small energy. High  $zT$  is also found in these systems such as [30]  $\text{La}_3\text{Te}_4$  and n type filled [67]  $\text{CoSb}_3$ .

An important aspect of band structure engineering is the idea of converging bands [68], where one manages to manipulate the position of a certain band extreme in the material to enable the multi-band/valley conduction.

In lead chalcogenides, the primary maximum of the valence bands is found at the L point of the First Brillouin Zone (FBZ) and a secondary maximum along the  $\Sigma$  line. The energy position of the L band depends on temperature and as T increases it shifts down. Thus the p type compounds will enter a multi-band conduction region where the highly degenerate ( $N_v = 12$ )  $\Sigma$  band plays an important role. This is based on the rigid band assumption which is found valid for p-type PbTe [69]. The complex

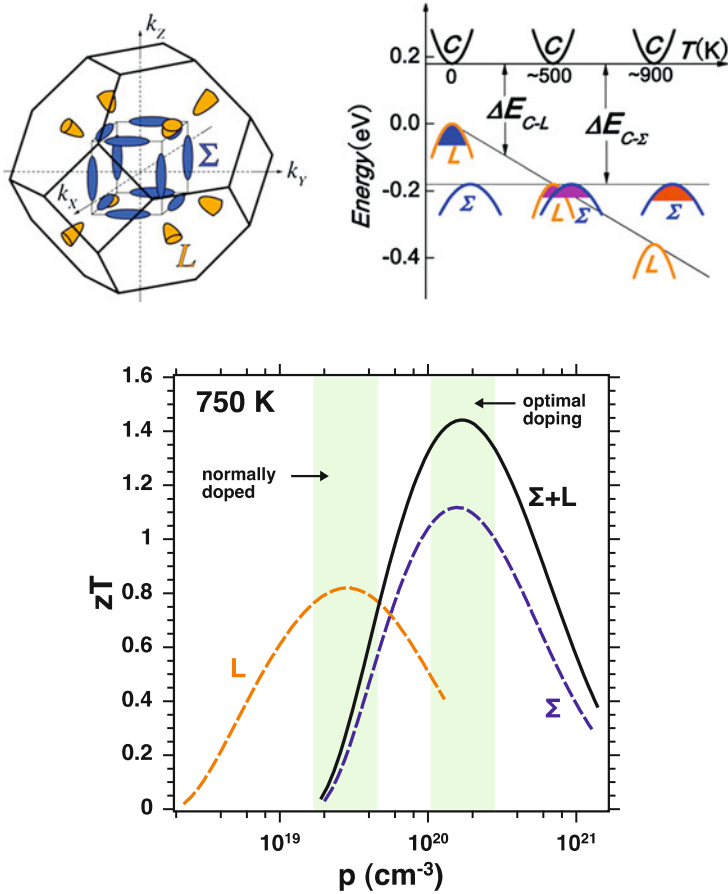


**Fig. 1.12** The schematic carrier pockets and band structure in p type PbTe. The calculation of  $zT$  indicates the  $zT$  of L and  $\Sigma$  band combined exceeds that of any single of them, which is believed to be the effect of higher  $N_v$

valence band structure explains why high  $zT > 1$  can be achieved in p type PbTe [70] and PbSe [71]. Moreover, the energy difference between L and  $\Sigma$  bands decreases when going from PbS to PbTe. Thus by alloying PbTe with other chalcogenides, the converging temperature can be manipulated so that the two bands are able to converge at a higher temperature. In this way, a higher  $zT$  of 1.8 was achieved in  $\text{PbTe}_{0.85}\text{Se}_{0.15}$  alloy [68] (Figs. 1.12).

The conduction band of  $\text{Mg}_2\text{X}$  (X: Si, Ge, Sn) is composed of a primary minimum at the X point of the FBZ. A secondary minimum is found above it at (roughly) the same k-point. In  $\text{Mg}_2\text{Si}$  the gap between its primary light band and the secondary heavy band [72] is  $\sim 0.4$  eV. In  $\text{Mg}_2\text{Sn}$ , the heavy band is lower in energy by  $\sim 0.2$  eV. These binary compounds are decent thermoelectrics with  $zT \sim 0.6$  (0.7 reported [73]).

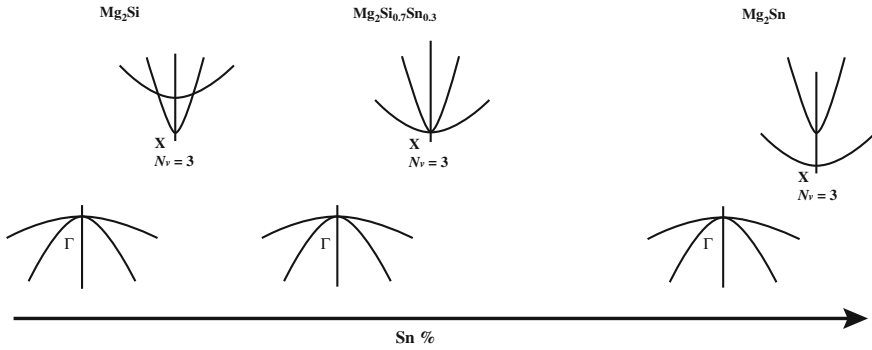


**Fig. 1.13** The schematic band structure of  $Mg_2Si$ - $Mg_2Sn$  alloys

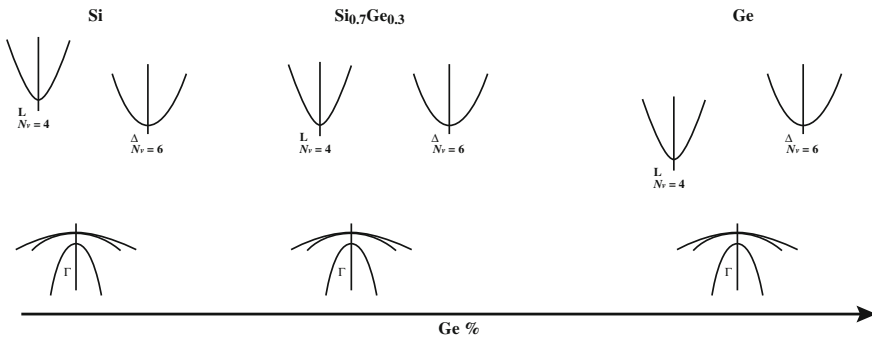


**Fig. 1.14** The schematic band structure of Si-Ge alloys

In  $Mg_2Si_xSn_{1-x}$  alloys the energy position of each band changes with  $x$  and converges when  $x$  is around 0.3 (Fig. 1.13) [72, 74, 75]. And it has been found [74, 76] that the highest  $zT$  is achieved for alloy with  $x$  value between 0.3 and 0.4 when the two band minimums are closed up.  $zT$  of 1.0 – 1.1 around 750 K has been reported by different groups [72, 77] (1.3 at 700 K according to recent report [74]). Even though the alloying would reduce thermal conductivity and increase  $zT$  such effect is less significant at high temperatures and tends to be compensated through the increased scattering of charge carriers. The two-band conduction is then a very important factor to achieve high  $zT$  in the  $Mg_2Si_xSn_{1-x}$  alloy.

$Si_{1-x}Ge_x$  provides another example of band convergence that increases  $N_v$ . Si and Ge, though similar in structure, are different in band configurations. The primary minimum of the conduction band in silicon is found along the zone center and X point ( $\Delta$ ) and the second minimum is at the L point (L). In germanium the band at the L point is the primary minimum while the  $\Delta$  band is found at a higher energy. Alloying silicon with germanium changes the energy position of L and  $\Delta$  valleys relative to the top of valence band and it has been found via both calculation [78] and transmission electron energy-loss spectroscopy [79] that they cross each other

around the composition of  $\text{Si}_{0.7}\text{Ge}_{0.3}$  (Fig. 1.14). This should be one of the reasons why  $\text{Si}_{0.8}\text{Ge}_{0.2}$  is useful as a good n type thermoelectric material [80–83].

## 1.7 Inter-band/Inter-valley Carrier Scattering

When Eqs. (1.11) and (1.16) were used to draw the conclusion that higher  $N_v$  is favorable for thermoelectrics, the scattering of carriers between different valleys (or bands when not equivalent in  $k$  space) was not taken into account. This could lead to a noticeable deviation between the actual  $zT$  and the  $zT$  one might expect from the simple model.

Depending on the position in  $k$  space of the initial and final states the scattering of carriers between them could have different nature. When two bands are located at the same  $k$  point, such as is the case in  $\text{Mg}_2\text{X}$  (X: Si, Ge, Sn), the scattering requires little change in electron wave vector, and thus, is of similar nature as intra-band scattering by acoustic phonons. Such inter-band scattering is accounted for in the framework of isotropic, parabolic band by Fedorov et al. [84, 85] in a form analogous to intra-band scattering:

$$\begin{aligned} \tau_{ac,1} = & \frac{\pi \hbar^4 C_{11}}{2^{1/2} m_1^{*3/2} (k_B T)^{3/2} \Xi_1^2} \varepsilon^{-1/2} \text{ when } \varepsilon < \Delta\varepsilon \\ & \left[ \left( \frac{\pi \hbar^4 C_{11}}{2^{1/2} m_1^{*3/2} (k_B T)^{3/2} \Xi_1^2} \varepsilon^{-1/2} \right)^{-1} \right. \\ & \left. + \left( \frac{\pi \hbar^4 C_{11}}{2^{1/2} m_2^{*3/2} (k_B T)^{3/2} D^2} (\varepsilon - \Delta\varepsilon)^{-1/2} \right)^{-1} \right]^{-1} \text{ when } \varepsilon > \Delta\varepsilon \end{aligned} \quad (1.28)$$

$$\begin{aligned} \tau_{ac,2} = & \left[ \left( \frac{\pi \hbar^4 C_{11}}{2^{1/2} m_2^{*3/2} (k_B T)^{3/2} \Xi_2^2} (\varepsilon - \Delta\varepsilon)^{-1/2} \right)^{-1} \right. \\ & \left. + \left( \frac{\pi \hbar^4 C_{11}}{2^{1/2} m_1^{*3/2} (k_B T)^{3/2} D^2} \varepsilon^{-1/2} \right)^{-1} \right]^{-1} \text{ when } \varepsilon > \Delta\varepsilon \end{aligned} \quad (1.29)$$

where  $\tau_{ac,1}$  and  $\tau_{ac,2}$  represents the relaxation time of carriers in the primary valley “1” and secondary valley “2”, separated by a reduced energy of  $\Delta\varepsilon$  (relative to the edge of the primary band, see Fig. 1.11), each is characterized by an effective mass of  $m_1^*$  and  $m_2^*$  and an intra-band acoustic phonon scattering deformation potential of  $\Xi_1$  and  $\Xi_2$ . The inter-band acoustic phonon scattering deformation potential  $D$

is the same regardless of the initial/final valley, has the same unit as  $\Xi$  and can be determined from functional calculation of interaction matrix elements.

The second term in Eqs. (1.28) and (1.29) has the same temperature and energy dependence as Eq. (1.16). As long as the inter-band deformation potential  $D$  is small compared to  $\Xi$  (roughly  $<30\%$ ), Eqs. (1.28) and (1.29) can be very well approximated using Eq. (1.16) with a slightly different  $\Xi$  value. However, it is difficult to estimate  $D$  in a compound without calculating the interaction matrix, thus it might be questionable to ensure that such an assumption is generally valid. Fedorov [84] estimated this inter-band scattering in  $\text{Mg}_2\text{Si}_{1-x}\text{Sn}_x$  alloys and found that up to 400 K the rate of inter-band scattering is on the order of  $10^{-3}$  of that of intra-band scattering, indicating the above assumption should hold for most cases.

Another case is for the scattering of carriers between equivalent valleys when the band extreme are not located at the center of FBZ. In this case a large change of the carrier's  $k$  vector is needed and the scattering process thus resembles that of the optical phonon scattering and is inelastic in nature [8, 17, 36, 38]. Herring studied the transport properties of semiconductors with multi-valley structure [8] and his result has been adopted by most of the relevant discussions. Herring wrote the total relaxation time  $\tau$  (under isotropic, parabolic band assumption) as:

$$\tau = \left\{ w_1 \left( \frac{E}{\hbar\omega} \right)^{1/2} \left( \frac{k_B T}{\hbar\omega} \right) + w_2 \left[ \frac{\left( \frac{E}{\hbar\omega} + 1 \right)^{1/2}}{\exp\left(\frac{\hbar\omega}{k_B T}\right) - 1} + \text{Re} \left( \frac{\left( \frac{E}{\hbar\omega} - 1 \right)^{1/2}}{1 - \exp\left(-\frac{\hbar\omega}{k_B T}\right)} \right) \right] \right\}^{-1} \quad (1.30)$$

The first term represents the intra-valley scattering process. The second term further contains two parts that represents the inter-valley phonon absorption and emission, respectively.  $\hbar\omega$  is the energy of phonons that participate the inter-valley scattering (hereinafter called inter-valley phonons). The momentum conservation requires these phonons to have large and (mostly) fixed wave vectors, which means the most contribution comes from high energy optical phonons that can be approximated with a constant energy  $\hbar\omega$ . Correspondingly there is a characteristic temperature  $\Theta_{\text{int}} = \hbar\omega/k_B$  which is lower than the optical phonon temperature (or Debye temperature). The factors  $w_1$  and  $w_2$  contains all the parameters that are not explicitly dependent on temperature or carrier energy, and the ratio  $w_2/w_1$  is used to characterize the relative intensity of inter-valley scattering to that of the intra-valley process.

Rewriting Eq. (1.30) and one can get:

$$\tau = \left\{ \frac{w_1}{(k_B \Theta_{\text{int}})^{3/2}} \varepsilon^{1/2} (k_B T)^{3/2} + w_2 (k_B T)^{1/2} \left[ \exp\left(\frac{\Theta_{\text{int}}}{T}\right) - 1 \right]^{-1} \right. \\ \left. [(\varepsilon + \Theta_{\text{int}}/T)^{1/2} + \exp(\Theta_{\text{int}}/T) \text{Re}((\varepsilon - \Theta_{\text{int}}/T)^{1/2})] \right\}^{-1} \quad (1.31)$$

In this form the second term can be easily recognized as an analog of Eq. (1.19) for the deformation potential scattering from optical phonons. And the first part shows the

same energy and temperature dependence as Eq. (1.16) for intra-band deformation potential scattering from acoustic phonons.

With the discussion above and within the context of high temperature ( $T > \Theta$ ) and heavily doped thermoelectrics (the temperature restriction would not be necessary if the degenerate limit is met), the influence of inter-valley scattering, same as the deformation potential scattering from optical phonons, will be included in Eq. (1.16) by using an effective deformation potential coefficient  $\Xi_{\text{eff}}$  [similar to the derivation of Eq. (1.23)]. It can be further predicted that when the intra-band deformation potential scattering from acoustic phonons dominates the other two mechanisms, this  $\Xi_{\text{eff}}$  shouldn't change much from  $\Xi_{\text{ac}}$  for the intra-band acoustic phonon scattering, which can be measured and related to  $\Xi_{\text{d}}$  and  $\Xi_{\text{u}}$ .

The magnitude of inter-valley transition can be probed by acoustic-electrical (piezoresistance) measurements [17], but convincing studies with comparison to the intra-valley process are very rare. Prediction of  $w_2/w_1$  is otherwise difficult without evaluating the interaction matrix. Nevertheless some important facts regarding the inter-valley process can be drawn from two relatively simple estimates: (1) whether the transition is allowed or forbidden, and (2) the characteristic temperature of the inter-valley phonons, which is comparable to the longitudinal optical phonon temperature or Debye temperature.

According to Fermi's golden rule, when the wave function of the initial and final electron state of a given transition are both odd (or even) functions the interaction matrix vanish and such a transition is forbidden. As an example, the primary conduction/valence band extreme of lead chalcogenides at the L point is described by the odd/even wave function [59] of  $L_6^-/L_6^+$  so that the inter-valley transition between equivalent L valleys is forbidden (however such restriction is weakened [36] when the nonparabolicity is taken into account and the corresponding states become a mixture of  $L_6^-$  and  $L_6^+$ ).

In a general context, a similar story is found in n-type germanium where the transition between conduction band minimums at the L point is found to be negligible [10, 86, 87].

The case of n-type silicon is rather complicated. One widely used result is that inter-valley scattering is important and [17, 88–90]  $w_2/w_1 = 2$ . The direct support of such claim is from the observed (drift) mobility  $\mu \sim T^{-2.5}$  in high purity n type Si [38, 86, 89, 91, 92] while the acoustic phonon scattering should only give a  $T^{-1.5}$  dependence. Based on Herring's theory, such a difference could be explained by considering inter-valley process with  $w_2/w_1 = 2$ . However, the original measurements done by Long, Morin, and Ludwig, where this  $T^{-2.5}$  relation is observed, were on very lightly doped (with dopant on order of  $10^{13} \text{ cm}^{-3}$ ) Si within the temperature range 30–400 K. Without ruling out the possibility of excitation of minority carriers (near room temperature) and the partial ionization of dopants (at low temperature) it may be risky to use the observed temperature dependence as evidence of inter-valley scattering. Moreover, Long [89] and Aubrey [90] concluded that the f type inter-valley scattering rate is two times that of the intra-valley scattering, which forms the main contribution for inter-valley scattering. These authors however also admitted that the characteristic temperature of inter-valley phonons for this f type

scattering is around 700 K, yet it is unexplained why the temperature dependence of mobility would change significantly even below room temperature when most of inter-valley phonon states are not populated. On the other hand, the mobilities found in Si with carrier density equal to [24] or above [83]  $10^{17} \text{cm}^{-3}$  at room temperature and above actually have the  $T^{-1.5}(T^{-1.3})$  dependence, which is just as expected from intra-valley deformation potential scattering processes.

Several more recent studies [37, 93–96] have calculated the inter-valley deformation potential of n type Si and the results vary from 2 to  $7 \times 10^8$  eV/cm. If the pre-factors in Eq. (1.21) are rewritten into the same form as in Eq. 1.16 (See Eq. 1.23) so that the values can be directly compared with  $\Xi_{\text{ac}}$ , these results will be equivalent to 1.3–4.6 eV, whereas the intra-valley acoustic phonon deformation potential is suggested [10, 37, 82, 83, 88] to be 7–9 eV (correspondingly the ratio  $w_2/w_1$  would be between 0.1 and 0.7, instead of 2). Such result indicates the inter-valley scattering is important but not dominant. For instance, assuming the “actual” inter-valley deformation potential is  $6 \times 10^8$  eV/cm and the intra-valley acoustic phonon deformation potential is 8 eV, then for degenerate samples the total relaxation time will still be well described using Eq. (1.16) with an effective deformation potential  $\Xi_{\text{eff}} = 9$  eV (Eq. 1.23).

In the more specific case of thermoelectric SiGe alloys, extensive modeling work [81–83, 88] has been able to excellently explain the observed transport properties of heavily doped SiGe alloys, without taking into account inter-valley scattering, and the deformation potentials  $\Xi$  used in these modeling are in good agreement with measured values. Which is another indication that the scattering from inter-valley and optical process is not comparable with the intra-valley acoustic process. Through first principle calculation, Murphy-Armando [97] predicted that for SiGe alloys with Si content up to 50% the former two processes combined only contribute to 1% of the total mobility at 300 K.

In the most conservative estimate, for the  $\text{Si}_{0.7}\text{Ge}_{0.3}$  alloy taking the inter-valley scattering into account and assuming  $w_2/w_1 = 2$ , Rowe [98] suggested a 40% reduction of the ratio  $zT_{\text{mv}}/zT_{\text{sv}}$  ( $zT_{\text{mv}}$ : maximum  $zT$  of a multi-valley system,  $zT_{\text{sv}}$ : maximum  $zT$  from a single valley of the same system) at 300 K caused by inter-valley scattering. This percentage would increase at higher temperature (70% at 1000 K estimated). To our knowledge there have not been any experimental or theoretical study that suggests a total compensation of the benefit from higher  $N_v$  due to the onset of inter-valley (inter-band) scattering.

## 1.8 Conclusion

The above sections present our recent understanding of the different physical parameters that go into the quality factor  $B$  that determines a material’s maximum  $zT$ . Identifying new structures with favorable combination of these parameters is one strategy of advancing thermoelectric research. For known materials, material engineering that leads to the improvement of  $B$  is important [99]. Most researchers

are familiar with the merit of  $\kappa_L$  reduction but aiming at other parameters should be equally promising. In PbTe there have been demonstrations of the concept of band structure engineering in various ways such as the valence band convergence tuning in the PbTe-PbSe alloy [68], the L valence band position manipulation in the PbTe-MgTe alloy [100] and the Fermi surface distortion in Tl contained PbTe or its alloys [101, 102].

Exploring the more fundamental linkage between the parameters in  $B$  is also important as these parameters are usually inter-related and the freedom of independently tuning one parameter without changing the others are likely limited.  $\kappa_L$  is often believed to be independently tunable, which is true when optimizing carrier density for maximum  $zT$  is the only concern. Such a view becomes plausible when further improvement is the target. An all-encompassing consideration of  $B$  is required towards achieving the state-of-the-art thermoelectric materials.

## References

1. R.P. Chasmar, R. Stratton, *J. Electron. Control* **7**, 52–72 (1959)
2. H.J. Goldsmid, *Introduction to Thermoelectricity* (Springer, Berlin, Heidelberg, 2010)
3. H.J. Goldsmid, *Thermoelectric Refrigeration* (Temple Press Books LTD, London, 1964)
4. G.S. Nolas, J. Sharp, H.J. Goldsmid, *Thermoelectrics Basic Principles and New Materials Developments* (Springer, Berlin, Heidelberg, 2001)
5. G.D. Mahan, *Solid State Physics*, (Academic Press Inc., San Diego, 1998), vol. 51, pp. 81–157
6. G.A. Slack, in *CRC Thermoelectric Handbook*, ed. by D.M. Rowe (CRC Press LLC, Boca Raton, 1995)
7. Y. Pei, A.D. LaLonde, H. Wang, G.J. Snyder, *Energy Environ. Sci.* **5**(7), 7963–7969 (2012)
8. C. Herring, *Bell Syst. Tech. J.* **34**(2), 237–290 (1955)
9. Y.I. Ravich, B.A. Efimova, I.A. Smirnov, *Semiconducting Lead Chalcogenides* (Plenum Press, New York, 1970)
10. C. Herring, E. Vogt, *Phys. Rev.* **101**(3), 944 (1956)
11. Y. Takagiwa, Y. Pei, G. Pomrehn, G. J. Snyder, *Appl. Phys. Lett.* **101**, 092102 (2012)
12. J. Bardeen, W. Shockley, *Phys. Rev.* **80**(1), 72 (1950)
13. E.S. Toberer, C.A. Cox, S.R. Brown, T. Ikeda, A.F. May, S.M. Kauzlarich, G.J. Snyder, *Adv. Funct. Mater.* **18**(18), 2795–2800 (2008)
14. A.F. May, E.S. Toberer, A. Saramat, G.J. Snyder, *Phys. Rev. B* **80**(12), 125205 (2009)
15. Y.I. Ravich, B.A. Efimova, V.I. Tamarchenko, *Phys. Status Solidi B-Basic Res.* **43**(2), 453–469 (1971)
16. L.G. Ferreira, *Phys. Rev.* **137**(5A), 1601–1609 (1965)
17. K. Seeger, *Semiconductor Physics An Introduction*, 9th edn. (Springer, Berlin, Heidelberg, 2004)
18. H. Wang, Y. Pei, A.D. LaLonde, G.J. Snyder, *Proc. Nat. Acad. Sci.* **109**(25), 9705–9709 (2012)
19. G.E. Pikus, G.L. Bir, *Sov. Phys. Solid State* **1**(11), 1502–1517 (1960)
20. G.L. Bir, G.E. Pikus, *Sov. Phys. Solid State* **2**(9), 2039–2051 (1961)
21. M.V. Fischetti, S.E. Laux, *J. Appl. Phys.* **80**(4), 2234–2252 (1996)
22. I.I. Zasavitskii, E. Silva, E. Abramof, P.J. McCann, *Phys. Rev. B* **70**(11), 115302 (2004)
23. H.Z. Wu, N. Dai, P.J. McCann, *Phys. Rev. B* **66**(4), 045303 (2002)
24. Springer Materials the Landolt-Börnstein Database
25. B.-L. Huang, M. Kaviani, *Phys. Rev. B* **77**(12), 125209 (2008)
26. T. Caillat, A. Borshchevsky, J.P. Fleurial, *J. Appl. Phys.* **80**(8), 4442–4449 (1996)

27. J.O. Sofo, G.D. Mahan, Phys. Rev. B **58**(23), 15620–15623 (1998)
28. J.L. Feldman, D.J. Singh, Phys. Rev. B **53**(10), 6273–6282 (1996)
29. A. May, J.-P. Fleurial, G. Snyder, Phys. Rev. B **78**(12), 125205 (2008)
30. A.F. May, D.J. Singh, G.J. Snyder, Phys. Rev. B **79**(15), 153101 (2009)
31. K. Tukioka, Jpn. J. Appl. Phys. Part 1 - Regul. Pap. Short Notes Rev. Pap. **30**(2), 212–217 (1991)
32. B.M. Askerov, *Electron Transport Phenomena in Semiconductors* (World Scientific Publishing Co. Pte. Ltd., Singapor, 1991)
33. D.J. Howarth, E.H. Sondheimer, Proc. Royal Society Lond. Ser. Math. Phys. sci. **219**(1136), 53–74 (1953)
34. V.W.L. Chin, R.J. Egan, T.L. Tansley, J. Appl. Phys. **69**(6), 3571–3577 (1991)
35. D.I. Bilc, S.D. Mahanti, M.G. Kanatzidis, Phys. Rev. B **74**(12), 125202 (2006)
36. L.Y. Morgovskii, Y.I. Ravich, Soviet Physics Semiconductors-Ussr **5**(5), 860 (1971)
37. C. Jacoboni, L. Reggiani, Rev. Mod. Phys. **55**(3), 645–705 (1983)
38. W.A. Harrison, Phys. Rev. **104**(5), 1281 (1956)
39. K. Takeda, N. Matsumoto, J. Phys. C-Solid State Phys. **17**(28), 5001–5015 (1984)
40. J.D. Wiley, M. Didomeni, Phys. Rev. B **2**(2), 427 (1970)
41. J.D. Wiley, Solid State Commun. **8**(22), 1865–1868 (1970)
42. M. Costato, G. Gagliani, C. Jacoboni, L. Reggiani, J. Phys. Chem. Solids **35**(12), 1605–1614 (1974)
43. Y.I. Ravich, Sov. Phys. Semiconductors-Ussr **3**(10), 1278 (1970)
44. R. Dalven, Phys. Rev. B **3**(6), 1953–1954 (1971)
45. H. Ehrenreich, J. Appl. Phys. **32**(10), 2155–2166 (1961)
46. D.L. Rode, Phys. Rev. B **2**(4), 1012–1024 (1970)
47. D.L. Rode, Phys. Rev. B-Solid State **2**(10), 4036–4044 (1970)
48. A.R. Hutson, Phys. Rev. **108**(2), 222–230 (1957)
49. Y.I. Ravich, B.A. Efimova, V.I. Tamarchenko, Phys. Status Solidi B-Basic Res. **43**(1), 11–33 (1971)
50. D.M. Zayachuk, Semiconductors **31**(2), 173–176 (1997)
51. C.M. Bhandari, D.M. Rowe, J. Phys. D: Appl. Phys. **18**(5), 873 (1985)
52. R.L. Petritz, W.W. Scanlon, Phys. Rev. **97**(6), 1620–1626 (1955)
53. S. Johnsen, J.Q. He, J. Androulakis, V.P. Dravid, I. Todorov, D.Y. Chung, M.G. Kanatzidis, J. Am. Chem. Soc. **133**(10), 3460–3470 (2011)
54. R.S. Allgaier, W.W. Scanlon, Phys. Rev. **111**(4), 1029–1037 (1958)
55. L.D. Zhao, S.H. Lo, J. He, H. Li, K. Biswas, J. Androulakis, C.I. Wu, T.P. Hogan, D.Y. Chung, V.P. Dravid, M.G. Kanatzidis, J. Am. Chem. Soc. **133**(50), 20476–20487 (2011)
56. H. Wang, E. Schechtel, Y. Pei and G. J. Snyder, Adv. Energy Mater. **3**, 488–498 (2013)
57. E.G. Bylander, M. Hass, Solid State Commun. **4**(1), 51–53 (1966)
58. Y. Kanai, K. Shohno, Jpn. J. Appl. Phys. **2**, 6–10 (1963)
59. Y. I. Ravich, in Lead Chalcogenides Physics and Applications, vol. 18, ed. by D. Khokhlov (Taylor and Francis, New York, 2003)
60. P. Ghosez, M. Veithen, J. Phys.-Condes. Matter **19**(9), 096002 (2007)
61. G. Kliche, Infrared Phys. **24**(2), 171–177 (1984)
62. G.S. Nolas, G.A. Slack, T. Caillat, G.P. Meisner, J. Appl. Phys. **79**(5), 2622–2626 (1996)
63. L. Chaput, J. Tobola, P. Pêcheur, H. Scherrer, Phys. Rev. B **73**(4), 045121 (2006)
64. P. Larson, S.D. Mahanti, M.G. Kanatzidis, Phys. Rev. B **62**(19), 12754–12762 (2000)
65. T.J. Zhu, K. Xiao, C. Yu, J.J. Shen, S.H. Yang, A.J. Zhou, X.B. Zhao, J. He, J. Appl. Phys. **108**(4), 044903–044905 (2010)
66. C. Yu, T.-J. Zhu, R.-Z. Shi, Y. Zhang, X.-B. Zhao, J. He, Acta Mater. **57**(9), 2757–2764 (2009)
67. X. Shi, J. Yang, J.R. Salvador, M.F. Chi, J.Y. Cho, H. Wang, S.Q. Bai, J.H. Yang, W.Q. Zhang, L.D. Chen, J. Am. Chem. Soc. **133**(20), 7837–7846 (2011)
68. Y. Pei, X. Shi, A. LaLonde, H. Wang, L. Chen, G.J. Snyder, Nature **473**(7345), 66–69 (2011)
69. Y. Takagiwa, Y. Pei, G. Pomrehn, G. J. Snyder, APL Materials in press (2013)
70. Y. Pei, A. LaLonde, S. Iwanaga, G.J. Snyder, Energy Environ. Sci. **4**, 2085–2089 (2011)

71. H. Wang, Y. Pei, A.D. Lalonde, G.J. Snyder, *Adv. Mater.* **23**(11), 1366–1370 (2011)
72. V.K. Zaitsev, M.I. Fedorov, E.A. Gurieva, I.S. Eremin, P.P. Konstantinov, A.Y. Samunin, M.V. Vedernikov, *Phys. Rev. B* **74**(4), 045207 (2006)
73. S.K. Bux, M.T. Yeung, E.S. Toberer, G.J. Snyder, R.B. Kaner, J.-P. Fleurial, *J. Mater. Chem.* **21**(33), 12259 (2011)
74. W. Liu, X. Tan, K. Yin, H. Liu, X. Tang, J. Shi, Q. Zhang, C. Uher, *Phys. Rev. Lett.* **108**(16), 166601 (2012)
75. X. Liu, H. Wang, L. Hu, H. Xie, G. Jiang, G. J. Snyder, X. Zhao, T. Zhu, *Adv. Energ. Mater.* doi:[10.1002/aenm.201300174](https://doi.org/10.1002/aenm.201300174) (2013)
76. D.A. Pshenay-Severin, M.I. Fedorov, *Phys. Solid State* **49**(9), 1633–1637 (2007)
77. Q. Zhang, J. He, T.J. Zhu, S.N. Zhang, X.B. Zhao, T.M. Tritt, *Appl. Phys. Lett.* **93**(10), 102109 (2008)
78. F. Ben Zid, A. Bhourri, H. Mejri, M. Said, N. Bouarissa, J.L. Lazzari, F.A. d'Avitaya, J. Derrien, *Physica B* **322**(3–4), 225–235 (2002)
79. P.E. Batson, J.F. Morar, *Appl. Phys. Lett.* **59**(25), 3285–3287 (1991)
80. X.W. Wang, H. Lee, Y.C. Lan, G.H. Zhu, G. Joshi, D.Z. Wang, J. Yang, A.J. Muto, M.Y. Tang, J. Klatsky, S. Song, M.S. Dresselhaus, G. Chen, Z.F. Ren, *Appl. Phys. Lett.* **93**(19), 193121 (2008)
81. M.N. Tripathi, C.M. Bhandari, *J. Phys. Condes. Matter* **15**(31), 5359–5370 (2003)
82. A.J. Minnich, H. Lee, X.W. Wang, G. Joshi, M.S. Dresselhaus, Z.F. Ren, G. Chen, D. Vashaee, *Phys. Rev. B* **80**(15), 155327 (2009)
83. G.A. Slack, M.A. Hussain, *J. Appl. Phys.* **70**(5), 2694–2718 (1991)
84. M. I. Fedorov, D. A. Pshenay-Severin, V. K. Zaitsev, S. Sano, M. V. Vedernikov, *Features of Conduction Mechanism in n-type Mg<sub>2</sub>Si<sub>1-x</sub>Sn<sub>x</sub> Solid Solutions*. (IEEE, New York, 2003)
85. D.A. Pshenay-Severin, M.I. Fedorov, *Phys. Solid State* **52**(7), 1342–1347 (2010)
86. H. Brooks, *Theory of the Electrical Properties of Germanium Silicon* (Academic Press Inc, NY, 1955)
87. W.P. Mason, T.B. Bateman, *Phys. Rev. Lett.* **10**(5), 151–154 (1963)
88. C.B. Vining, *J. Appl. Phys.* **69**(1), 331–341 (1991)
89. D. Long, *Phy. Rev.* **120**(6), 2024–2032 (1960)
90. J.E. Aubrey, W. Gubler, T. Henningsen, S.H. Koenig, *Phys. Rev.* **130**(5), 1667–1670 (1963)
91. F.J. Morin, J.P. Maita, *Phys. Rev.* **96**(1), 28–35 (1954)
92. G.W. Ludwig, R.L. Watters, *Phys. Rev.* **101**(6), 1699–1701 (1956)
93. J.G. Nash, J.W. Holmkennedy, *Phys. Rev. B* **15**(8), 3994–4006 (1977)
94. P.D. Yoder, V.D. Natoli, R.M. Martin, *J. Appl. Phys.* **73**(9), 4378–4383 (1993)
95. S.V. Obukhov, V.G. Tyuterev, *Phys. Solid State* **51**(6), 1110–1113 (2009)
96. Z. Wang, S. D. Wang, S. Obukhov, N. Vast, J. Sjakste, V. Tyuterev, N. Mingo, *Phys. Rev. B* **83**(20), 205208 (2011)
97. F. Murphy-Armando, S. Fahy, *Phys. Rev. B* **78**(3), 035202 (2008)
98. D.M. Rowe, C.M. Bhandari, *J. Phys. Lett.* **46**(1), L49–L52 (1985)
99. H. Wang, A.D. LaLonde, Y. Pei, and G. J. Snyder, *Adv. Funct. Mater.* **23**, 1586–1596, (2013)
100. Y. Z. Pei, A. D. LaLonde, N. A. Heinz, X. Y. Shi, S. Iwanaga, H. Wang, L. D. Chen, G. J. Snyder, *Adv. Mater.* **23**(47), 5674–5678 (2011)
101. J.P. Heremans, V. Jovovic, E.S. Toberer, A. Saramat, K. Kurosaki, A. Charoenphakdee, S. Yamanaka, G.J. Snyder, *Science* **321**(5888), 554–557 (2008)
102. C.M. Jaworski, B. Wiendlocha, V. Jovovic, J.P. Heremans, *Energy Environ. Sci.* **4**, 4155–4162 (2011)



<http://www.springer.com/978-3-642-37536-1>

Thermoelectric Nanomaterials  
Materials Design and Applications  
Koumoto, K.; Mori, T. (Eds.)  
2013, XIX, 387 p., Hardcover  
ISBN: 978-3-642-37536-1